North American glaciations and Pacific inputs in the Nd and Sr isotope Pleistocene record from the western Arctic Ocean

Jesse M. Muratli[1], Leonid Polyak[2], Brian A. Haley[1], and Anton Kuznetsov[3]

[1]College of Earth, Ocean, and Atmospheric Sciences, Oregon State University, Corvallis, OR, USA, [2]Byrd Polar and Climate Research Center, The Ohio State University, Columbus, OH, USA, [3]Institute of Precambrian Geology and Geochronology, Russian Academy of Sciences, St. Petersburg, Russian Federation.

Corresponding author: Jesse M. Muratli (jesse.muratli@oregonstate.edu)

Key Points:

- We measured strontium and neodymium isotope ratios on the leached, lithogenic fractions of a sediment core from the Western Arctic.
- The sediment record covers the past 3.3 million years of change in the Arctic, a critical and understudied time period in this region.
- Prolonged closures of the Bering Strait are key components to the intensification of glacial cycles after the Mid-Pleistocene Transition.

Abstract

Enduring questions remain regarding the transition from relatively warm and stable pre- and early-Pleistocene climate to that of the high amplitude glacial-interglacial cycles later in the Quaternary. The main shift in glacial intensity and periodicity around 1 Ma is known as the Mid Pleistocene Transition (MPT). Here we analyze detrital strontium (Sr) and neodymium (Nd) isotopes in a Western Arctic sediment core P23 previously investigated using several litho/biostratigraphic proxies. Based on an improved age framework combining lithostratigraphic cyclicity and Sr isotope stratigraphy, the P23 record extends to ~3.3 Ma, thus providing a rare insight into the Quaternary Arctic climate change. The distinct pre-MPT P23 record is dominated by Pacific-sourced sediment inputs, with little to no intra-Arctic glacial inputs except for a sandy interval around ~2.5 Ma. A consistent decrease of Nd isotopic values towards North American glacigenic signature started in both the Arctic and Bering Sea at ~1.5 Ma and led to a major threshold shift in P23 proxies at ~0.9 Ma. We argue that this threshold is associated with the first prolonged closure of the Bering Strait for an entire obliquity cycle. This shift marks the expansion of the North American ice sheets to the Arctic margin, with dramatic impacts on depositional and hydrographic environments in the Arctic Ocean. These impacts strengthened in the subsequent glacial intervals indicating further ice-sheet growth, probably fed back by continuing prolonged Bering Strait closures. Potential implications of these Arctic changes for the evolution of North Atlantic circulation require further investigation.

Plain Language Summary

A significant change in Earth's climate system, the Mid-Pleistocene Transition (MPT), happened around one million years ago and caused ice ages to become longer and colder. To improve our understanding of this transition we analysed the elements strontium (Sr) and neodymium (Nd) in a marine sediment core from the Western Arctic Ocean. Based on this and previous work done on the same core we show that material mostly came from the south through the Bering Strait in the first half of our record. Around 1.5 million years ago the isotopic ratios of Sr and Nd in our core indicate an increasing contribution of material from the North American continent, building to the MPT when larger

sediment grains abruptly appear; an indication of massive ice sheet growth and a resulting discharge of icebergs into the Arctic Ocean. We argue that this major change happens the first time the Bering Strait was closed– due to the drop in sea level caused by the growth of ice on land– through an interglacial period. After this event, subsequent massive ice sheets and prolonged Bering Strait closures worked together to create longer and colder glacial periods than were seen before the MPT.

1. INTRODUCTION

Late Cenozoic climate change is characterized by a long-term cooling trend overprinted with glacial-interglacial cycles (Zachos et al., 2001). This cyclicity was paced on a 41-ka orbital obliquity period until the Mid-Pleistocene Transition (MPT; ~1250–700 ka) when glacial cycles shifted to a dominant 100-ka period (P. U. Clark et al., 2006; Elderfield et al., 2012). The cause for the shift in glacial periodicity during the MPT is not completely understood, and has been attributed to various factors such as a fall in atmospheric pCO_2 (Hönisch et al., 2009), growth of Antarctic ice sheets (Elderfield et al., 2012), or progressive glacial erosion of the North American regolith (P. U. Clark & Pollard, 1998). Studies of the MPT in the Northern Hemisphere focus primarily on continuous records from the North Atlantic (Hodell et al., 2008; Pena & Goldstein, 2014; Poirier & Billups, 2014) or Pacific (Kender et al., 2018; Knudson & Ravelo, 2015). Recent data constrain the timing of the main MPT shift to ca. 0.9-1 Ma in both regions (Kender et al., 2018; Yehudai et al., 2021) The latter study, based on the strontium (Sr) and neodymium (Nd) isotopic data from the North Atlantic, offers greatest support for the regolith hypothesis (Yehudai et al., 2021).

An obvious gap in knowledge on this critical paleoclimate shift lies with the Arctic Ocean that connects the North Atlantic and Pacific oceans and is a major depocenter for products of circum-Arctic glacial erosion. To date, Arctic Ocean paleoclimate studies have dealt mainly with the most recent glacial cycles typically recovered by sediment cores (Fagel et al., 2014; Jakobsson et al., 2000; Löwemark et al., 2013) or the long Cenozoic record with large stratigraphic gaps (Darby, 2008; Haley, Frank, Spielhagen, & Eisenhauer, 2008; Haley, Frank, Spielhagen, & Fietzke, 2008; Moran et al., 2006). The first study of the Arctic Ocean Quaternary history with a focus

on the MPT utilized sediment core P1-93AR-P23 (P23 hereafter) from the Northwind Ridge, located relatively close to both the Bering Strait and the Pleistocene Laurentide Ice Sheet (LIS) margin (Fig. 1) (Dipre et al., 2018; Polyak et al., 2013). These works demonstrate a dramatic MPT change in litho- and biostratigraphy that was related to the onset of large North American glaciations and the spread of perennial sea ice. Here we advance these insights into the Arctic Ocean evolution during and beyond the MPT by analyzing lithogenic Sr and Nd isotopic data from the same sediment core (P23). The data generated are interpreted in the context of potential isotopic sources as well as other Pleistocene records in the Arctic, North Pacific, and North Atlantic oceans. A comparison of these records indicates that the MPT climatic and sea-level changes modulated the Bering Strait throughflow, which had a major effect on Arctic glaciations and on the paleoceanography of the western Arctic Ocean. We argue that especially large glacial volumes and extents in the Arctic North America were enabled by extended closures of the Bering Strait during and after the MPT.

2. SETTINGS

2.1. Study area.

The study site is located near the northern end of the Northwind Ridge that extends into the Canada Basin from the Chukchi-Alaskan margin north of the Bering Strait (Fig. 1). Present hydrographic, sea-ice, and depositional conditions in this area are primarily controlled by the clockwise, wind-driven Beaufort Gyre circulation that can deliver sediments from the North American margin. However, the configuration and strength of the Beaufort Gyre, and the concurrent Transpolar Drift circulation, can vary with changes in atmospheric circulation, and could have been considerably different in the past (Bischof & Darby, 1997; Dong et al., 2020; Stärz et al., 2012). As shown by a multiproxy study of middle to upper Quaternary sediments from the P23 area (Wang et al., 2021), deposition in this region during glacial intervals was predominated by glacigenic inputs from North America by way of icebergs or meltwater. In comparison, interglacial sediments transported mainly by sea ice have more affinity to the Chukchi-East Siberian continental margin (Rong Wang et al., 2021). The latter sources can have a considerable contribution from the Bering Strait inflow that exerts a strong control over

111 circulation and sediment dynamics on the Chukchi shelf (Yamamoto et al., 2017). In
112 addition to the surface circulation, the top of the Northwind Ridge is impacted by a mid-
113 depth current that is likely forced by the Atlantic water flowing into the Arctic (Atlantic
114 Intermediate Water) (Dipre et al., 2018; Wang et al., 2021). While the depth of P23 site at
115 ~950 mwd is somewhat below the modern range of Atlantic Intermediate Water, it was
116 likely affected by past changes in Arctic intermediate circulation related to climate and
117 sea-level variations.
118

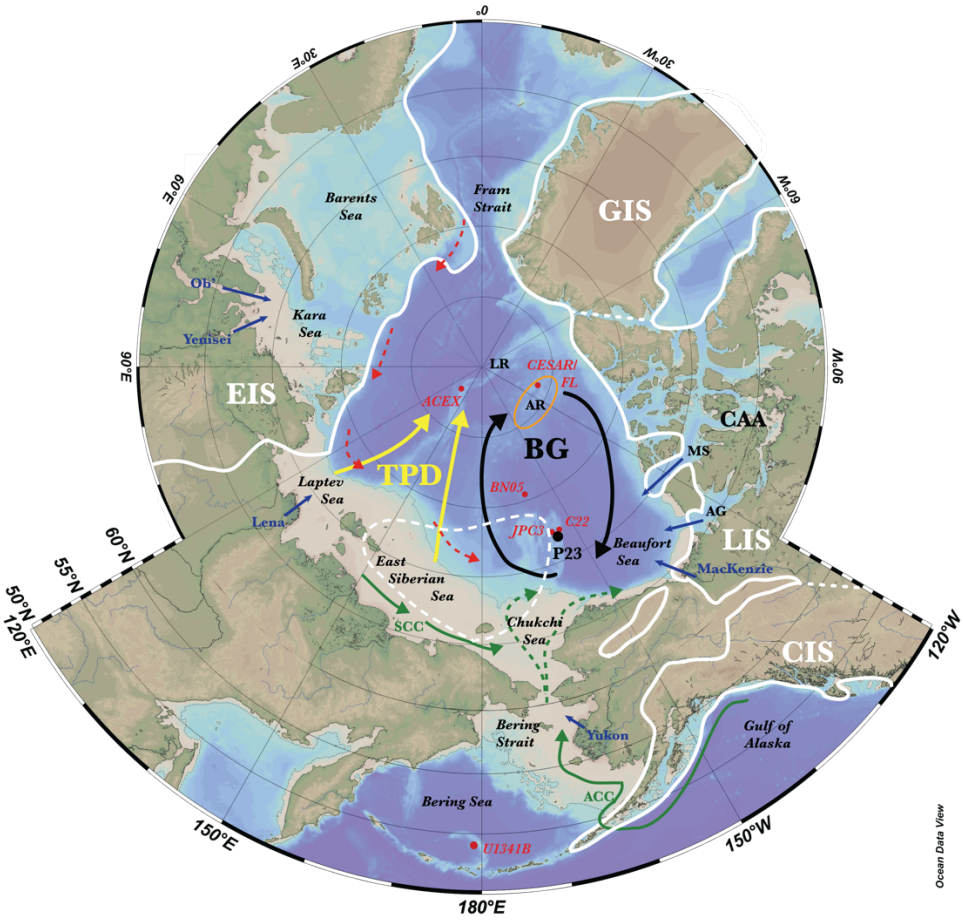

Figure 1. Index map of the Arctic Ocean and Bering Sea. Core sites: P23 - black, other cores used in the text - red. Alpha Ridge (AR) sites are outlined in orange. Yellow and black arrows show major surface circulation features: Transpolar Drift (TPD) and Beaufort Gyre (BG), respectively. Green arrows – shelf currents: dotted – Bering Strait inflow, SCC – Siberian Coastal Current, ACC – Alaska Coastal Current. Red dotted arrows - Atlantic Intermediate Water flow. White outlines show the inferred maximum extent of Pleistocene glaciations around the Arctic Ocean (Dyke et al., 2003; Kaufman et al., 2011; Svendsen et al., 2004); dotted line for more hypothetical East Siberian Ice Sheet (Niessen et al., 2013). EIS, CIS, LIS, GIS – Eurasian, Cordilleran, Laurentide, and Greenland Ice Sheets. Blue arrows – major rivers. CAA - Canadian Arctic Archipelago; AG - Amundsen Gulf; MS - M'Clure Strait. AR, LR – Alpha and Lomonosov Ridges

2.2. Isotopic tracers.

Isotopic composition of radiogenic elements such as Sr and Nd (Wasserburg et al., 1981) are being increasingly used as provenance tracers in Arctic sediments for paleoclimate and circulation reconstruction (Asahara et al., 2012; Fagel et al., 2014; Hillaire-Marcel et al., 2013; Porcelli et al., 2009; Winter et al., 1997). Of those studies, only the data of Winter et al. (1997) and Haley et al. (2008a) extend beyond the MPT, but the stratigraphic coverage of these records is very sparse. Furthermore, the material for these isotope studies was derived from a variety of sediment components (e.g., bulk sediment, only fine/coarse grains, or leachate residues), thus complicating data comparisons, especially considering potential grain-size related offsets in the isotopic composition (Eisenhauer et al., 1999; Tütken et al., 2002; Rong Wang et al., 2021). Such offsets notably affect Sr isotopes, while εNd data appear to be more consistent (Borg & Banner, 1996).

Arctic sediment provenances show a wide range of detrital isotopic compositions, including Nd and Sr isotopes (Dong et al., 2020; Fagel et al., 2014), making them powerful proxies for circum-Arctic paleoenvironments and circulation. Most of the North American material represents eroded Canadian Shield and adjacent platform rocks characterized by distinctly unradiogenic (more negative) ε_{Nd} and high $^{87}Sr/^{86}Sr$ values (McCulloch & Wasserburg, 1978). The opposite pattern in the Sr-Nd isotopic composition, showing more radiogenic (less negative) ε_{Nd} and lower $^{87}Sr/^{86}Sr$ values, can originate from several sources including igneous rocks from Siberia, a few outcrops in Alaska, and the North Pacific inflow via the Bering Strait (e.g. (Asahara et al., 2012; Lightfoot et al., 1993; Sharma et al., 1992; Tikhomirov et al., 2008; Wooden et al., 1993)). Variation in these sources has been useful for reconstructing western Arctic paleoceanography during several last glacial-interglacial cycles, including records from the western Arctic Ocean with a moderate stratigraphic resolution (cm/kyr) (Fig. 1; cores BN05 and C22) (Dong et al., 2020; Rong Wang et al., 2021).

3. MATERIALS AND METHODS

Piston core P23 was collected in 1993 aboard the US Coast Guard vessel *Polar Star.* Core stratigraphy and prior analytical results are reported in earlier studies (Polyak

et al., 2009, 2013). Similar to other stratigraphic Arctic Ocean studies (Cronin et al., 2013; O'Regan et al., 2008), the age model for the Upper to Middle Pleistocene (<0.8 Ma) was based on relating explicit lithostratigraphic cycles and events in the upper ~160 cm of the core to Marine Isotope Stages (Polyak et al., 2009, 2013). The lower, more visually homogeneous part of the core, was dated using Sr isotopes measured on benthic foraminifera (Dipre et al., 2018). For more detailed age constraints, we performed 6 additional Sr isotope measurements (Suppl. Table 1) using the same methods and facilities as in Dipre et al. (2018).

For sediment isotope geochemistry, core P23 was sampled every 2 to 10 cm for the upper 100 cm and every 10 to 25 cm thereafter to the core bottom at 527 cm. Sediments had previously been sequentially leached with buffered acetic acid and hydroxylamine HCl (Haley, Frank, Spielhagen, & Fietzke, 2008), and the remaining lithogenic fractions were digested using a microwave (CEM MARS-5) (Muratli et al., 2012). For Ca and Mn elemental composition we use XRF records generated earlier (Polyak et al., 2013), as the leaching process most likely affected the concentrations of these elements in our samples.

A portion of each digest was passed through chromatographic columns to separate and purify Sr and Nd (Abbott et al., 2016), and the isotopic ratios of the isolated elements were measured using a Nu Plasma multi-collector ICP-MS at Oregon State University. Strontium isotopes were normalized to $^{86}Sr/^{88}Sr$ of 0.1194 and corrected using NBS 987 ($^{87}Sr/^{86}Sr = 0.710245$). An in-house standard (EMD) gives a 2-sigma external reproducibility of ±0.000027 (n = 46). Neodymium isotopes were normalized to $^{146}Nd/^{144}Nd = 0.7219$. The JNdi-1 standard was used for correction (reference $^{143}Nd/^{144}Nd$ value of 0.512115 ±0.000007, (Tanaka et al., 2000)), and an in-house standard (SpecPure) gives a 2σ external reproducibility of ±0.000016 (n = 53). JNdi-1 and SpecPure were analyzed every 6 samples and analyzed in replicate at the beginning and end of every batch run. Neodymium isotopes are denoted by ε_{Nd}, which is the deviation of measured $^{143}Nd/^{144}Nd$ to a Chonritic Uniform Reservoir (CHUR; $^{143}Nd/^{144}Nd = 0.512638$, (Wasserburg et al., 1981)): $\varepsilon_{Nd} = [(^{143}Nd/^{144}Nd_{meas} / 0.512638) - 1] * 10^4$.

194 To illustrate the extent of interconnectivity between the Pacific and the Arctic
195 (thus Atlantic) Ocean over the 40-ka and 100-ka orbital cycles, we modeled a simple
196 Bering Strait Throughflow Index (BSTI) reflecting the open/closed status of the strait
197 through time. We used 50 m as an approximation for the sill depth of the modern Bering
198 Strait, such that when sea level falls below this, the Pacific–Arctic connection is cut off.
199 No correction was applied for potential glacioisostatic influence, which has been
200 negligible since the last glaciation (Jakobsson et al., 2017; Spada & Galassi, 2017),
201 although we cannot exclude the possibility of a larger isostatic effect related to older
202 glaciations. We assigned a value of zero to each time point when global sea level was
203 lower than 50 m below modern and a value of one when the sea level was above this
204 level, based upon the reconstructions of Elderfield et al. (2012) and (Rohling et al.,
205 2014). We then determined the proportion of the previous obliquity or eccentricity cycle
206 that the Bering Strait was open by calculating a running average over the preceding 40 ka
207 or 100 ka (Suppl. Table 2).
208
209 **4. RESULTS**
210 **4.1. Litho- and biostratigraphy**.
211 Core P23 litho- and biostratigraphy has been presented in Polyak et al. (2013)
212 with additions in Dipre et al. (2018). The primary feature of the core is a distinct division
213 between a visually homogeneous, brown, mostly fine-grained sediment below ~165 cm
214 and interlamination of brown and grey intervals with a considerable amount of coarse
215 material above (Units 2 and 1, respectively). Unit 2 is characterized by low amounts of
216 coarse grains (>63 μm), mostly below 5% with a modest increase in the interval between
217 ~350 and 450 cm (Fig. 2). This unit also has variable but overall high Mn and negligibly
218 low Ca content. In comparison, Unit 1 shows cyclic peaks of coarse grains up to almost
219 40% co-varying with high Ca values, increasing up-core, that is inversely related to Mn
220 content. Polyak et al. (2013) have demonstrated that the boundary between units 1 and 2
221 also corresponds to a turnover in foraminiferal and ostracod fauna, where many species
222 thriving in Unit 2 environments got suppressed or went completely extinct.
223

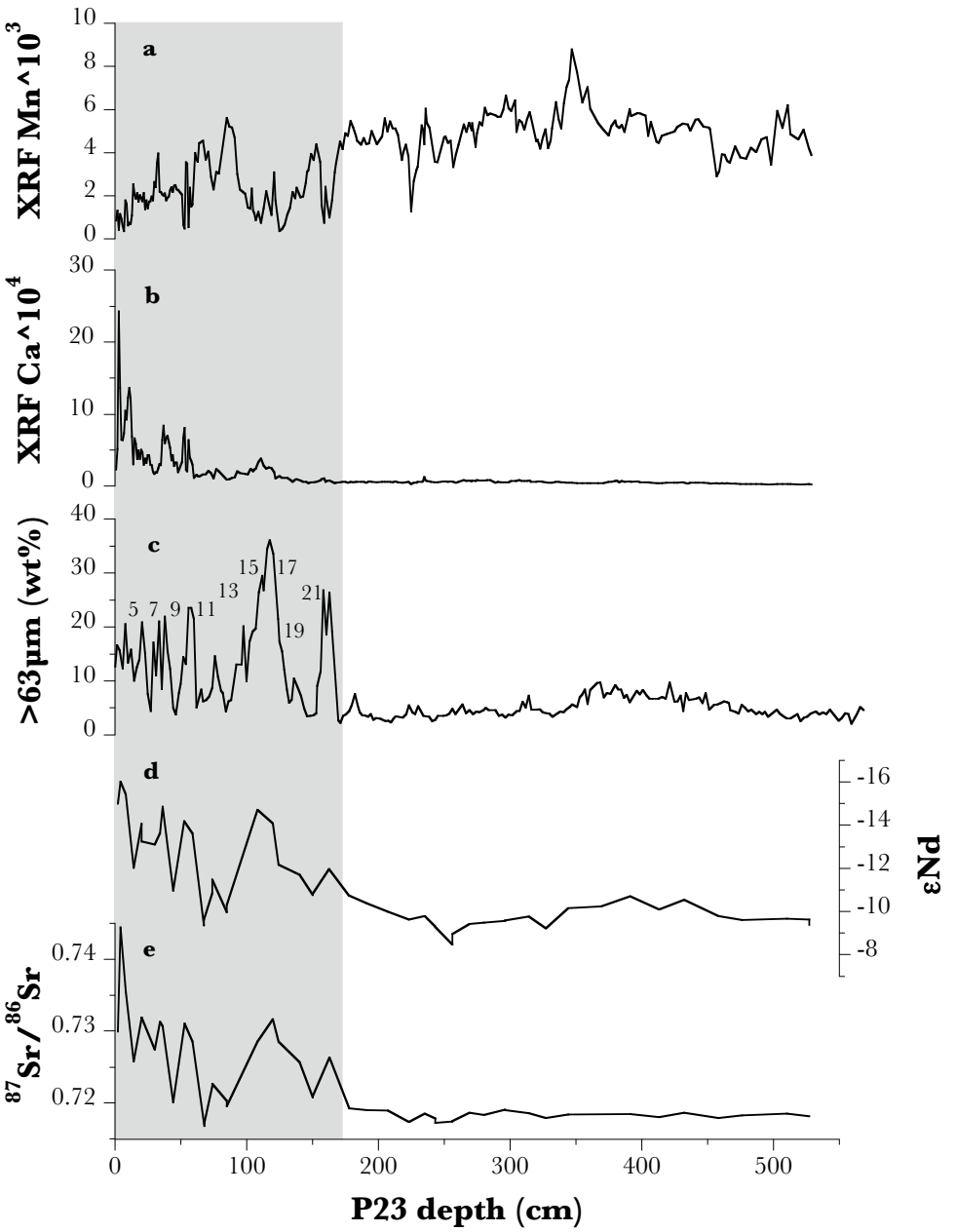

Figure 2. P23 proxies vs. core depth. (a-b) XRF content of (a) Mn and (b) Ca, and (c) sand content >63µm (wt %) (Polyak et al., 2013); (d-e) detrital isotopes (d) εNd and (e) $^{87}Sr/^{86}Sr$ (this study). Lithostratigraphic Unit 1 is shaded. Interglacial MIS are marked above the sand curve in Unit 1 as in Polyak et al. (2013).

230 **Table 1:** *Strontium and neodymium isotope data from detrital fractions of leached*
231 *sediment, core P23*
232

Core depth (cm)		Age (Ma)	$^{86}Sr/^{87}Sr$	$^{143}Nd/^{144}Nd$	ε_{Nd}
2-3		0.073	0.729927	0.511870	-15.0
4-5		0.079	0.744358	0.511818	-16.0
8-9		0.092	0.735456	0.511848	-15.4
14-15		0.112	0.725786	0.512022	-12.0
20-21		0.140	0.731714	0.511919	-14.0
20-21	***(rpt)***	***0.140***	***0.731832***	***0.511960***	***-13.2***
30-31		0.217	0.727420	0.511967	-13.1
34-35		0.231	0.731294	0.511940	-13.6
36-37		0.238	0.730625	0.511877	-14.8
44-45		0.277	0.720109	0.512076	-11.0
52.5-53.5		0.349	0.731038	0.511911	-14.2
58.5-59.5		0.389	0.728476	0.511940	-13.6
67.5-68.5		0.400	0.716772	0.512159	-9.3
67.5-68.5	***(rpt)***	***0.400***	***0.717256***	***0.512145***	***-9.6***
73.5-74.5		0.415	0.722262	0.512083	-10.8
73.5-74.5	***(rpt)***	***0.415***	***0.722686***	***0.512050***	***-11.5***
84.5-85.5		0.493	0.720255	0.512127	-10.0
84.5-85.5	***(rpt)***	***0.493***	***0.719549***	***0.512111***	***-10.3***
108-109		0.585	0.728516	0.511885	-14.7
119.5-120.5		0.618	0.731595	0.511917	-14.1
124-125		0.637	0.728480	0.512015	-12.2
140-141		0.746	0.725621	0.512039	-11.7
150-151		0.783	0.720792	0.512087	-10.7
150-151	***(rpt)***	***0.783***	***0.720939***	***0.512084***	***-10.8***
162.5-163.5		0.810	0.726347	0.512025	-12.0
177.5-178.5		0.978	0.719209	0.512088	-10.7
191-192		1.068	0.718985	0.512107	-10.4
207-208		1.175	0.718933	0.512127	-10.0
223-224		1.282	0.717374	0.512145	-9.6
235-236		1.362	0.718515	0.512137	-9.8
243-244		1.416	0.717826	0.512162	-9.3
243-244	***(rpt)***	***1.416***	***0.717219***	***0.512163***	***-9.3***
256-257		1.503	0.717444	0.512205	-8.5
256-257	***(rpt)***	***1.503***	***0.717494***	***0.512179***	***-8.9***
269-270		1.589	0.718641	0.512156	-9.4
280-281		1.663	0.718291	0.512153	-9.5
296-297		1.770	0.719040	0.512149	-9.5
296-297	***(rpt)***	***1.770***	***0.718962***	***0.512147***	***-9.6***
314-315		1.890	0.718547	0.512138	-9.8
327-328		1.977	0.717902	0.512166	-9.2

Core depth (cm)		Age (Ma)	$^{86}Sr/^{87}Sr$	$^{143}Nd/^{144}Nd$	ε_{Nd}
344-345		2.090	0.718403	0.512118	-10.1
369-370		2.257		0.512114	-10.2
391-392		2.404	0.718455	0.512090	-10.7
413-414		2.551	0.718042	0.512121	-10.1
432-433		2.678	0.718638	0.512098	-10.5
458-459		2.852	0.717888	0.512136	-9.8
476-477		2.972	0.718277	0.512147	-9.6
510-511		3.199	0.718512	0.512144	-9.6
527-528		3.313	0.718134	0.512145	-9.6
527-528	***(rpt)***	***3.313***	***0.718133***	***0.512158***	***-9.4***

4.2. Age model.

Following the approach from earlier P23 studies (Dipre et al., 2018; Polyak et al., 2013; Rujian Wang et al., 2018), we constrain the age for Unit 1 using lithostratigraphic cycles expressed in Mn and sand content variability and verified by several stratigraphic events (Fig. 3). This approach is consistent with other core stratigraphies from the central Arctic Ocean including the long IODP record from the Lomonosov Ridge (e.g., (O'Regan et al., 2008; Polyak et al., 2009; Stein, Matthiessen, Niessen, et al., 2010). Due to a more homogeneous lithostratigraphy and potentially different controls on the Mn distribution in the underlying Unit 2, the age framework for these sediments is based on Sr isotope stratigraphy (SIS) as in Dipre et al. (Fig. 3) (2018). A best-fit linear regression approximates Sr dates with an R^2=0.96, omitting apparent outliers. Due to a considerable data spread and inherent SIS uncertainties (McArthur et al., 2012), the resulting age model is inevitably approximate. Nevertheless, it makes good paleoclimatic sense and appears to be consistent with other regional stratigraphic records, as discussed in Section 5 below. Considering the caveats, the overall age model results in average sedimentation rates of 2.1 and 1.5 mm/kyr in Units 1 and 2, respectively, consistent with low deposition in the central part of the western Arctic Ocean covered by heavy sea ice (Polyak et al., 2009; Stein, Matthiessen, Niessen, et al., 2010). While these sedimentation rates indicate low stratigraphic resolution of core P23, they allow for a relatively deep stratigraphic coverage with the estimated core bottom age of ca. 3.3 Ma ka (upper Pliocene).

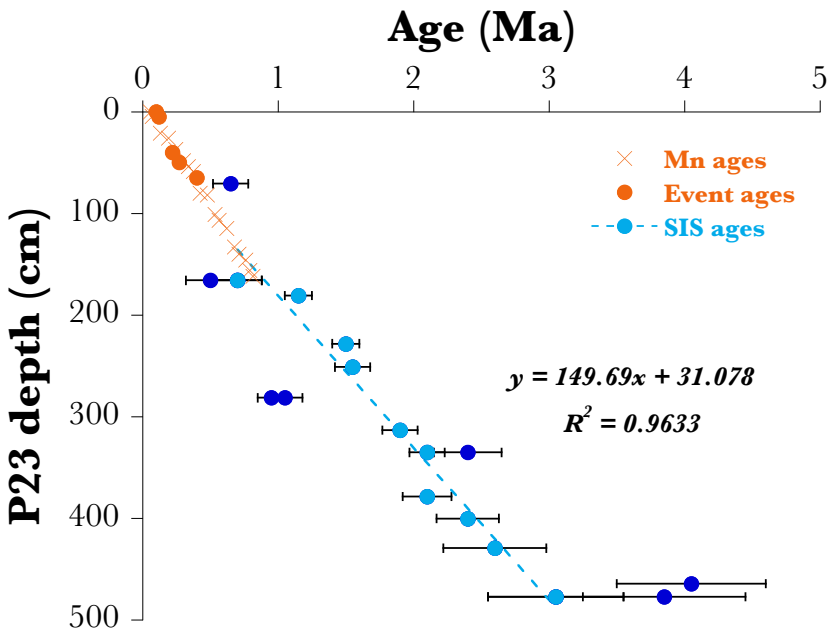

Figure 3. Age model for P23. Age is constrained by Mn tuning and event ages in Unit 1 (Polyak et al., 2013, Dipre et al., 2018) and by SIS ages below (Dipre et al., 2018, and new data). Dark blue dots represent SIS outliers not included in the age model.

4.3. Isotopic data.

Unit 2 is consistently characterized by overall low $^{87}Sr/^{86}Sr$ and high ε_{Nd} values (above -10 and below 0.72, respectively), with a modest decrease in ε_{Nd} in a coarser-grained interval between ~350 and 450 cm (Fig. 2). The first spike in coarse grains at the bottom of Unit 1 is associated with elevated $^{87}Sr/^{86}Sr$ and more negative ε_{Nd} (0.726 and -12, respectively). A similar isotopic signature marks all the coarse peaks in Unit 1, with $^{87}Sr/^{86}Sr$ getting overall higher (to 0.744) and ε_{Nd} more negative (to -16), while finer-grained intervals in Unit 1 have isotopic signatures more like those of Unit 2. To enable the interpretation of the isotopic results and comparison with Arctic/North Pacific potential provenance sources, we plotted the data in a Sr-Nd space with data points from Units 2 and 1 marked by different symbols (Fig. 4).

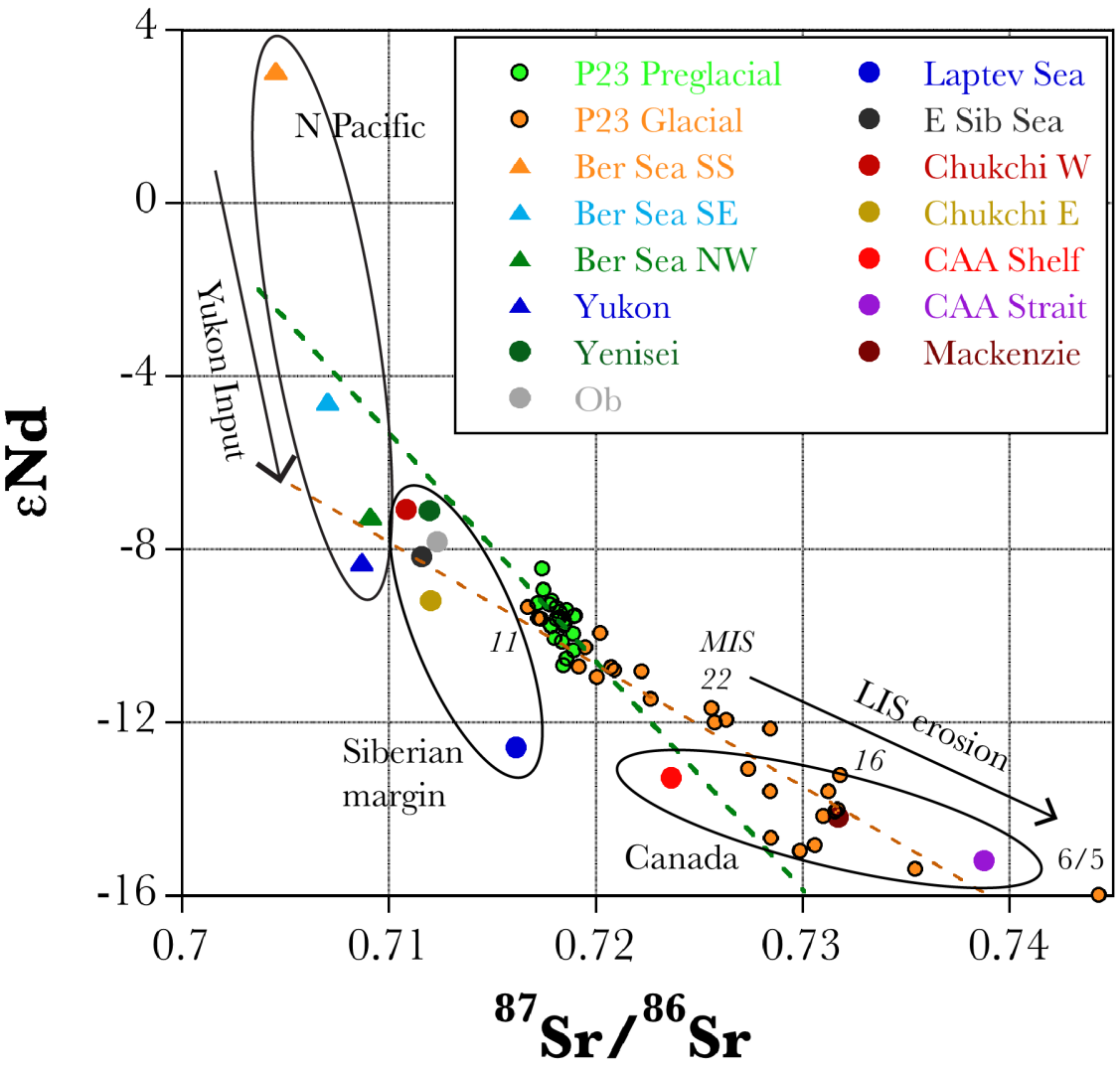

Figure 4. Distribution of the P23 and potential source data in εNd -$^{87}Sr/^{86}Sr$ space. Small orange and green circles show P23 samples from Units 1 and 2 respectively (see Fig 2). MIS numbers are indicated for several prominent glacial stages. Larger circles and triangles show source data from rivers and shelf areas of the Arctic and N Pacific, respectively (Asahara et al., 2012; Maccali et al., 2018; Xiao et al., 2021); see also Suppl. Table 3. Major geographic source groups (N Pacific, Siberian margin, and Canadian Arctic) are shown by ellipses. Ber – Bering, E Sib – East Siberian, CAA – Canadian Arctic Archipelago.

5. DISCUSSION

5.1. Sediment provenance and depositional environments.

Downcore isotopic distributions need to be interpreted in the context of other sedimentary proxies and regional isotopic tracer data. The most telling feature of our results is a strong linkage between the isotopic and other stratigraphic data. The pronounced litho- and biostratigraphic boundary between units 2 and 1 is also expressed in a distinct shift in isotopic values (Fig. 2). This change, estimated to have occurred in the MPT at ca. 0.9-0.95 Ma, has been interpreted as a transition from relatively stable lower Pleistocene (preglacial) environments with seasonal sea ice and low glacial inputs to strong periodic glacial controls and perennial sea ice thereafter (Dipre et al., 2018; Polyak et al., 2013). In addition to mostly low sand content, high Mn and very low Ca composition, Unit 2 has low $^{87}Sr/^{86}Sr$ and relatively high (radiogenic) ε_{Nd} values (Fig. 2). Moderate variations in sand content, including a sandy interval at ~350-450 cm, appear to be inversely related to the ε_{Nd} record. The inverse co-variation between ε_{Nd} and sand is even more pronounced in Unit 1, which also has cyclic coarse-grained peaks with low Mn and high, increasing up-core Ca contents. Along with Ca, $^{87}Sr/^{86}Sr$ values show an increasing trend during consecutive glacial intervals in Unit 1. This co-occurrence of the grain-size with elemental and isotopic tracer proxies indicates a concerted change in Arctic paleoenvironments, provenance sources and circulation.

Finer grained sediments are typically delivered to the interior of the Arctic Ocean by sea ice from suspension on shallow continental shelves (Dethleff, 2005; Nürnberg et al., 1994). Larger, mostly sand-sized grains (>63 μm) are generally delivered by icebergs or in some cases by anchor ice (D.L. Clark & Hanson, 1983; Darby et al., 2011). Sediments with greater proportion of sand-sized and coarser grains, especially in the intervals related to glaciations, are interpreted as an increase in iceberg inputs (O'Regan et al., 2008; Polyak et al., 2009; Stein et al., 2012). Similar to the North Atlantic (e.g., Hodell et al., 2008), coarse-grained layers in the Arctic Ocean records are typically interpreted as glacial instability events (Polyak et al., 2009; Stokes et al., 2005; Rong Wang et al., 2021).

Elemental proxies provide a first assessment of provenance for sediment contributions from various circum-Arctic sources. As the Arctic Ocean has little biogenic

sedimentation, the Ca content of sediment is highly sensitive to input from carbonaceous rocks, primarily from the dolomitic terranes of the western Canadian Arctic Archipelago (CAA) (Bazhenova et al., 2017; Polyak et al., 2009). While in modern sediments dolomite deposition is mostly proximal to the major sources on the Banks and Victoria Islands (Gamboa et al., 2017), during glacial intervals dolomitic material was widely distributed by icebergs (Bazhenova et al., 2017; Polyak et al., 2009). In contrast to detrital Ca that is related to glacial erosion, Mn in Quaternary Arctic Ocean sediments appears to be primarily associated with inputs from continental margins during interglacials (Löwemark et al., 2013; Yurco et al., 2010). Another factor in sedimentary Mn variations, especially apparent in preglacial sediments of Unit 2, has been related to variability in bottom currents controlled by sea-level changes (Dipre et al., 2018).

The Sr-Nd composition in Arctic Ocean sediments is typically distributed between high-$^{87}Sr/^{86}Sr$, low ε_{Nd}, and low-$^{87}Sr/^{86}Sr$, high ε_{Nd} values, representing cratonic North American rocks and magmatic sources in Siberia or North Pacific, respectively (Dong et al., 2020; Rong Wang et al., 2021; Xiao et al., 2021). While generally P23 data are distributed in Sr-Nd isotopic space similarly to other records, there are significant differences between data from Units 1 and 2 (Fig. 4). The range of isotope values in Unit 2 is much more restricted and shifted towards low-$^{87}Sr/^{86}Sr$, high-ε_{Nd} values as compared to the Unit 1 data. Furthermore, the slope of the regression lines for data from units 1 and 2 is considerably different.

The high-$^{87}Sr/^{86}Sr$/low-ε_{Nd} data typical for coarse-grained samples of both Units point toward North American sources representing mainly crustal terrains of the Canadian Shield and the fringing platform rocks (Fig. 4) (Maccali et al., 2018; McCulloch & Wasserburg, 1978) (see Dong et al. (2020) and Wang et al. (2021) for a more comprehensive source overview). Data from glacial intervals in Unit 1 trend towards the CAA inter-island and McKenzie River areas. This signature becomes more pronounced in younger glaciations (middle to upper Pleistocene). In comparison, moderately coarse-grained samples from the sandy interval in Unit 2, trend towards a more mixed isotopic composition trending towards modern sediments from the CAA shelf (Maccali et al., 2018).

On the other, non-CAA end of the $^{87}Sr/^{86}Sr$-ε_{Nd} distribution, data from both Units trend towards Chukchi/East Siberian or North Pacific provenances (Fig. 4). Unit 2 data indicate a strong contribution from young igneous rocks characteristic for the southern Bering Sea (Asahara et al., 2012). Interglacial data from Unit 1 are more comparable to the Chukchi/East Siberian margin and the northern Bering Sea, the source of the modern Bering Strait inflow that includes considerable input from the Yukon River (Asahara et al., 2012; Maccali et al., 2018). Some of the interglacial data show a contribution from North American provenances, which we argue reflects mixing during transport, as in modern environments (Dong et al., 2020; Rong Wang et al., 2021).

5.2. Arctic glaciation and circulation history.

The isotopic record for most of P23 Unit 1 is generally similar to higher resolution isotopic records from the western Arctic Ocean (Fig. 1; cores BN05 and C22) (Dong et al., 2020; Rong Wang et al., 2021). Regardless of the potential compatibility issues with material used in these records (coarse grains or bulk sediment, respectively), they both show high-$^{87}Sr/^{86}Sr$/low-ε_{Nd} compositions in glacial intervals and low-$^{87}Sr/^{86}Sr$/high-ε_{Nd} values in interglacial sediments.

The two Arctic isotopic studies extending below the MPT include a composite record from several cores from the Alpha Ridge (AR) (Winter et al., 1997) and an IODP ACEX record from the Lomonosov Ridge (LR) (Chen et al., 2012; Haley, Frank, Spielhagen, & Eisenhauer, 2008) (Fig. 1). In modern conditions, these locations are predominantly influenced by the Beaufort Gyre and the TransPolar Drift circulations, respectively. The stratigraphic coverage of these samples is very sparse, except for a younger Pleistocene part of the LR study. For comparison purposes, an earlier suggested AR age model was adjusted to match the estimated ages of the LR and our samples using the same lithostratigraphic approach as in (Stein, Matthiessen, & Niessen, 2010) and similarities in the sand curves from P23 and the primary AR record CESAR-11 (David L. Clark et al., 1990).

The comparison of LR and AR pre-MPT records with that of P23 Unit 2 shows general similarity in the down-core ε_{Nd} distribution with some scatter due to uncertainties in the age models (Fig. 5). The LR data have a consistent offset of up to 2 units towards

lower ε_{Nd} values relative to P23, and the AR data show a slightly smaller offset in the lowermost (Pliocene) sediments underlying the sandy interval. These offsets may indicate differences in source sediment entrainment and/or transportation modes and pathways. Considering the existing circulation system, it is likely that under non-glacial conditions LR sedimentation was primarily controlled by sea-ice transport from the central Siberian margin, resulting in ε_{Nd} values trending towards the Laptev Sea signature (Fig. 5). In comparison, correlative data from the AR, affected by the Beaufort Gyre, are more likely reflective of input from North American sources. The resulting offset from the Pliocene P23 data may indicate different limbs of the Beaufort Gyre circulation delivering material from different parts of the Chukchi-CAA margin, as discussed in Wang et al. (2021). A narrower gap between the AR and P23 ε_{Nd} values in the lower Pleistocene sandy interval is consistent with a change of the P23 sources towards greater CAA contributions (Fig. 4). This change suggests the likelihood of growing ice-sheet(s), which would deliver

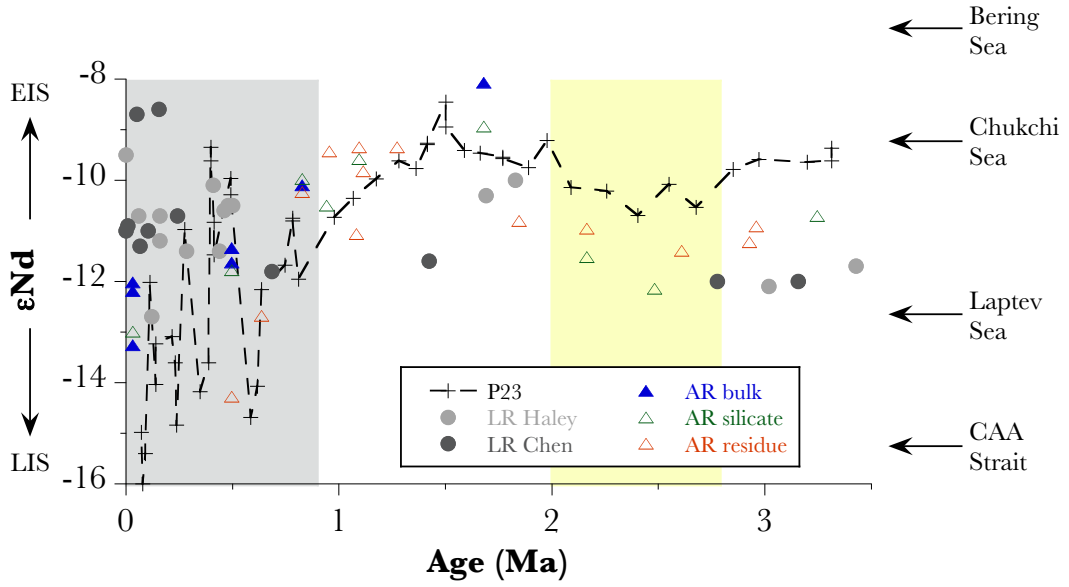

Figure 5. Comparison of detrital εNd records from P23, Lomonosov Ridge (LR, circles), and Alpha Ridge (AR, triangles). Grey and yellow fields show P23 Unit 1 and the sandy interval in Unit 2. Age for the AR samples is adjusted to the age model for P23 and LR. εNd composition for glacial and shelf sources is marked on the left and right, respectively. LIS, EIS - Laurentide and Eurasian Ice Sheets. LR data from (Haley, Frank, Spielhagen, & Fietzke, 2008) and (Chen et al., 2012); AR data from (Winter et al., 1997).

coarse CAA material to the margin with subsequent transport of this sediment by icebergs and/or sea ice. Very low Ca (dolomite) content and relatively low $^{87}Sr/^{86}Sr$ values in this interval (Fig. 2) indicate that the development of large ice sheets comparable to those later in the Pleistocene was not likely. As the Bering Strait remained open due to overall high Early Pleistocene sea level, the Pacific input at that time was not restricted, resulting in a mixed sediment signature in the study area.

The stratigraphic interval above the sandy layer contains the highest ε_{Nd} values in all three records (Fig. 5). This maximum ε_{Nd} probably indicates an especially strong Pacific input affecting circulation and sediment distribution in the central Arctic Ocean. The more detailed P23 record shows two ε_{Nd} maxima at ca. 1.5 and 2 Ma, compared to ε_{Nd} peak in the AR and LR data between these times. This difference may reflect age model inaccuracies and lack of sampling resolution, although a factor of circulation complexity cannot be ruled out. The AR and LR ε_{Nd} peaks appear to be co-eval with maximal current impact on the Northwind Ridge top at ca. 1.8-1.9 Ma (core JPC3; Fig. 1) that is indicative of intensified mid-depth circulation (Dipre et al., 2018). The interval above ca. 1.5 Ma shows a consistent decrease in ε_{Nd} values to the top of Unit 2 in both P3 and the AR record (no data for the LR). More detailed comparison records are needed for comprehending the Early Pleistocene Arctic circulation system.

Unit 1 in P23 shows high variance between glacial/interglacial intervals with contrasting low/high ε_{Nd} values, below and above the value of -12, respectively. The sparse AR data appear to have a similar variance. In contrast, the overall high (mostly above -12) ε_{Nd} data in the LR record have an opposite pattern with very high ε_{Nd} values during the glacial intervals, especially in the Upper Pleistocene. This contrast implies a strong divergence in glacial sources for sediments from the western Arctic Ocean and LR, provided by the LIS and the Eurasian Ice Sheet (EAIS), respectively (Fig. 1). While in modern-type conditions sedimentation on the LR is mostly controlled by the TransPolar Drift originating from the Laptev and East Siberian seas, during glaciations a stronger cyclonic circulation may have resulted in greater sediment delivery from west Siberia (Dong et al., 2020; Rong Wang et al., 2021; Xiao et al., 2021). This provenance constitutes a distinct ε_{Nd}-$^{87}Sr/^{86}Sr$ signature from the eroded west Siberian rocks (Lightfoot et al., 1993; Sharma et al., 1992; Wooden et al., 1993), manifested in some of

the glacial intervals in sediment records across the Arctic Ocean (Dong et al., 2020; Rong Wang et al., 2021). Unfortunately, P23 lacks most of the upper Pleistocene sediments to test the presence of the west Siberian material identified on the Northwind Ridge in MIS 4 (Rong Wang et al., 2021).

5.3. Broader paleoclimatic context.

5.3.1. Late Pliocene to MPT culmination

A continuous Plio-Pleistocene ε_{Nd} record from the southern Bering Sea (IODP core U1341B: (Horikawa et al., 2015)) provides much needed context for Arctic-North Pacific interaction in comparison with P23 (Fig. 6). Due to inaccuracies in the age models, the comparison may not be perfect, but the overall correspondence between the records appears to be convincing, especially for the pre-MPT. The upper Pliocene ε_{Nd} records in both U1341B and P23 show a gradually decreasing isotopic signature, indicative of the initiation of glacial inputs. This trend culminates in both cores in a lower Pleistocene ε_{Nd} minima centered at ca. 2.5 Ma in the stratigraphic interval of the sandy layer in P23 (Fig. 6, blue field). This correspondence indicates a considerable glacial impact on both the North Pacific and the Arctic Ocean, consistent with significant North American glaciation in the earliest Pleistocene, around 2.5 Ma (Balco & Rovey II, 2010; Shakun et al., 2016). It has been suggested that this glaciation may have started with the growth of the Cordilleran Ice Sheet (CIS) due to a sustained moisture supply from the North Pacific (Hidy et al., 2013). In turn, the CIS had a strong cooling effect on the North Pacific (Studer et al., 2012) and impacted sediment supply to the Bering Sea through iceberg discharge (Krissek, 1995) and re-routing of the Yukon River (Duk-Rodkin et al., 2001).

Our data from P23 provide the first indication that this Early Pleistocene glaciation resulted in ice sheet(s) at the Arctic North American margin ~~as well~~. The grain size and ε_{Nd} evidence points to an ice-sheet extent that reached the Arctic Ocean coasts, and thus could be comparable to later glaciations. However, based on the moderate number of coarse grains, very low Ca (dolomite) content, and relatively low $^{87}Sr/^{86}Sr$ values in this interval (Fig. 2), we infer this glaciation was not voluminous enough to erode CAA bedrock. In addition to sedimentary glacigenic proxies, this early glacial

458 interval features a pronounced decline in foraminiferal numbers and the first Pleistocene
459 extinction affecting part of the assemblage (Fig. 6) (Polyak et al., 2013). This event likely
460 reflects an abrupt decrease in biological production in relation to glacial meltwater inputs
461 and/or expansion of perennial ice.
462 After a subsequent return to non-glacial conditions in both the Bering Sea and the
463 western Arctic, another dip in the ε_{Nd} values appears in the U1341B data (Fig. 6),
464 possibly indicating another CIS expansion. The correlative feature in the P23 ε_{Nd} record
465 is more subtle and is not accompanied by elevated sand content. However, this interval
466 also corresponds to increased winnowing on the Northwind Ridge top at ~1.8-1.9 Ma
467 (Dipre et al., 2018), which could mask coarse grain numbers by redeposited fines.
468 A steady, long-term decrease of ε_{Nd} values started synchronously in both records
469 at ca. 1.5 Ma, indicating an increase in glacigenic sedimentary inputs. The expansion of
470 North American ice would be consistent with a widespread cooling that changed the
471 circulation pattern in the North Atlantic at ~1.6 Ma (Khélifi & Frank, 2014) and an
472 intensified glacial erosion revealed in the seawater Sr isotopes since ~1.5 Ma (Fig. 6, blue
473 field) (Yehudai et al., 2021). However, ice sheet extent to the Arctic coastline at this time
474 is not likely, given the lack of increase in sand content in P23 that would be indicative of
475 iceberg transport. We infer that glacigenic sediment was probably transported by glacial
476 runoff either directly into the Arctic Ocean or via the Bering Sea.
477

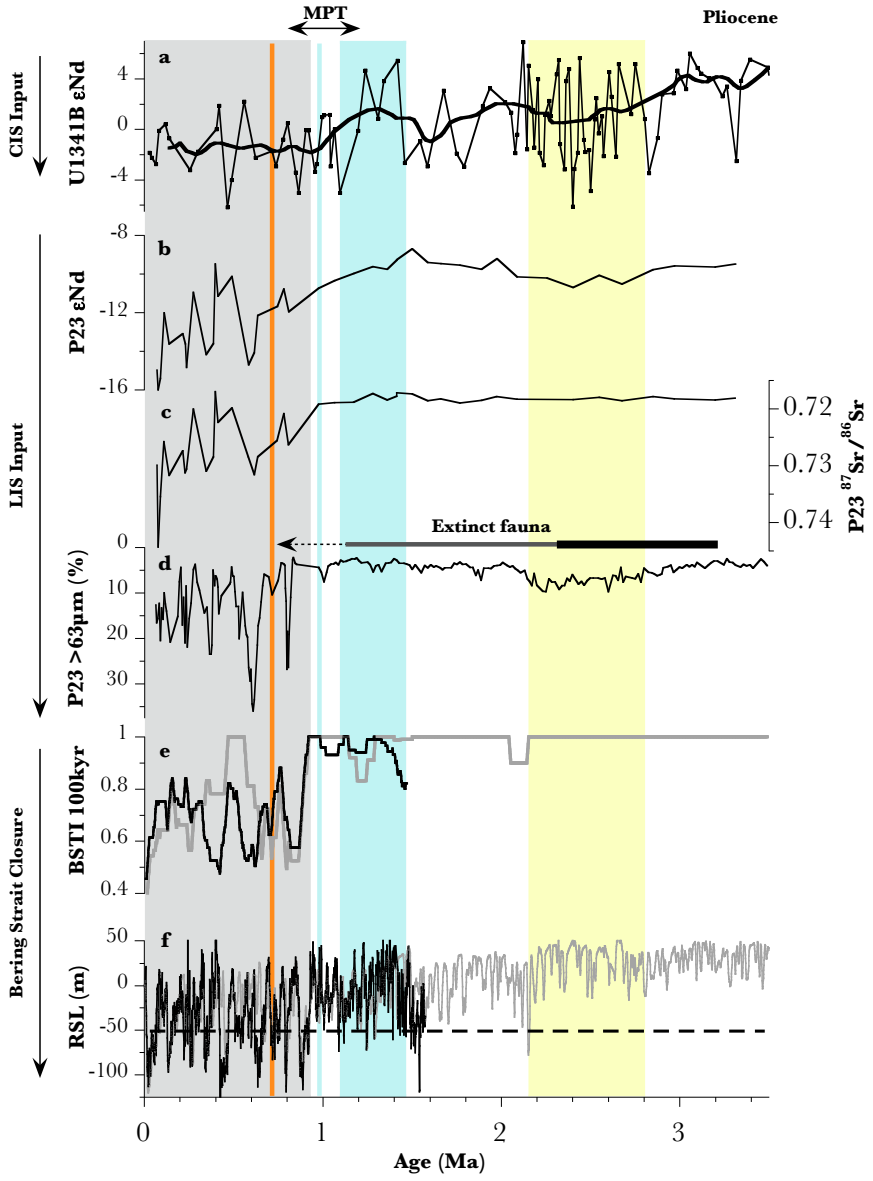

Figure 6. Paleoclimatic context for P23 record. (a) εNd data from the Bering Sea core U1341B (Fig. 1) with 400 ky running mean (Horikawa et al., 2015); (b-d) P23 data for (b) εNd, (c) $^{87}Sr/^{86}Sr$ (reverse), and (d) sand content (reverse) (Polyak et al., 2013, and this study); (e) Bering Strait Throughflow Index (this study), 100-ky average based on (f) Relative Sea Level from Elderfield et al., 2012 (black) and Rohling et al., 2014 (grey) (see also Suppl. Table 2). Dashed line in the RSL panel – Bering Strait sill depth, -50 m. Yellow field - sandy interval in P23 Unit 2; blue field and line - seawater $^{87}Sr/^{86}Sr$ change and detrital εNd shift in the N Atlantic (Yehudai et al., 2021); orange line - onset of detrital Ca input in P23 (Polyak et al., 2013). Extinct benthic fauna range from Polyak et al. (2013); changes in line thickness mark major extinction events.

The relatively gradual climatic deterioration starting from ~1.5 Ma led to the profound MPT shift in predominant orbitally-driven glacial cycles from 41-kyr to ~100-kyr (P. U. Clark et al., 2006; Elderfield et al., 2012). The MPT change involving further cooling and lowering sea level obviously affected the North Pacific and the Arctic, as corroborated by our data (Fig. 6). A rapid reduction in ε_{Nd} values as well as surface temperature/salinity indicators, both reflecting enhanced glacial inputs, started in the Bering Sea at the MPT onset ~1.2-1.3 Ma (Horikawa et al., 2015). This timing precedes pronounced MPT changes in the North Atlantic (Yehudai et al., 2021) and in the P23 record (Fig. 6), which suggests that Northern Hemisphere glacial expansion may have started with the CIS, similar to an earlier glacial interval in the lower Pleistocene (Hidy et al., 2013; Studer et al., 2012). This climatic pattern is consistent with the leading role of glaciations and related circulation changes in the North Pacific demonstrated for late Pleistocene millennial-scale climate events (Walczak et al., 2020).

Further increases in the proxies of glacial inputs continue to MIS 22 (~0.87-0.9 Ma) in both the Bering Sea and P23 records (Fig. 6). The latter shows the strongest shift in both the average values and the range of isotopic ratios up to this point, along with a sharp rise in coarse-grain content. This abrupt change most likely marks a threshold expansion of the North American glaciers to the Arctic margin. On the other hand, subdued Ca levels (Fig. 2) indicate that glacial erosion was not yet deep enough to impact the CAA bedrock with dolomitic rocks. The delayed exhaustion of the regolith in the Arctic in comparison with the Atlantic side of the LIS (~0.95-0.97 Ma: Yehudai et al., 2021) would be consistent with slower development of the northwestern LIS sector, as modelled for later Pleistocene glaciations (Batchelor et al., 2019; Kleman et al., 2013). In any case, a pronounced increase in glacial inputs in P23 at estimated MIS 22 provides the first evidence of the MPT ice-sheet expansion in the Arctic.

Kender et al. (2018) suggested that a threshold MPT sea-level drop at MIS 22 (Elderfield et al., 2012) was responsible for circulation change and sea-ice expansion in the Bering Sea via the closure of the Bering Strait. Arguably, a closed Bering Strait for a prolonged period should have also profoundly affected the Arctic Ocean via deprivation of relatively warm Pacific inflow (Shimada et al., 2006). Polyak et al. (2013) proposed that a litho/ biostratigraphic shift observed in P23 between units 1 and 2 was related to

the MPT decrease in Pacific inflow. We further evaluate this scenario by the Bering Strait Throughflow Index (BSTI; see Methods above). Zero BSTI values based on RSL after Elderfield et al. (2012) are first seen in MIS 24 around 0.92 Ma and, after a brief partial recovery, in MIS 22 for as long as 30 kyr, ~0.87-0.9 Ma. This appears to be the first prolonged closure of the Bering Strait lasting for an almost entire obliquity cycle (Fig. 6, S1). We suggest that the corresponding threshold change in the isotope composition and grain size in the western Arctic Ocean reflects a feedback between a prolonged closure of the Bering Strait and growth of massive glaciers in northern North America. This paleoclimatic mechanism implies that the Bering Strait gateway exerts a major control over the climatic evolution of the Arctic.

5.3.2. Late to post-MPT development

The subsequent Middle to Late Pleistocene history of Arctic glaciations is characterized by an enhanced LIS signature in sedimentary isotopic composition (Figs. 2, 6), indicating more extensive and/or deeper glacial erosion of the cratonic North American rocks. This trend is not observed in the Bering Sea data that show relatively stable glacial isotopic ratios since MIS 22, indicating no increase in CIS inputs (Fig. 6) (Horikawa et al., 2010, 2015; Jang et al., 2017). We infer that this Pacific-Arctic difference is related to the continuing effect of prolonged Bering Strait closures on the Arctic climate and hydrology.

A pronounced late/post-MPT change in the P23 record is the major faunal turnover in the foraminiferal fauna along with a strong decrease in sedimentary Mn content at MIS 18, both indicating perennial sea-ice growth in the western Arctic Ocean (Figs. 2, 6) (Polyak et al., 2013). This event is followed by the sharp increase in detrital Ca content at the onset of MIS 16, ~0.65 Ma (Fig. 2; Fig. 6, orange line). Detrital Ca input indicates the beginning of significant glacial erosion of dolomitic rocks in the western CAA (Bazhenova et al., 2017; Polyak et al., 2009; Rong Wang et al., 2021), as is supported by a concurrent intensification of glacial isotopic signature (higher $^{87}Sr/^{86}Sr$, lower ε_{Nd} values) and a maximum peak of coarse-grained material (Figs. 2, 6). This glacial event in P23 appears to be co-eval with the onset of LIS detrital carbonate pulses to the North Atlantic known as the Heinrich Events (Hodell et al., 2008). This

correspondence of glacial discharge events in both the Arctic and Atlantic suggests that a deepening erosion on the northwestern and eastern side of the LIS may indicate a major step in its overall growth, potentially making the ice sheet inherently unstable.

The profound changes in ice-sheet and sea-ice conditions during MIS 16-18 can be attributed to continuing late/post-MPT Bering Strait closures. Based on the BSTI, such closures extended over a total of ~20 kyr at MIS 18 (around 0.72 Ma) and >40 kyr at MIS 16 (~0.66-0.62 Ma) (Fig. 6, S1). The latter closure, comparable to the threshold MPT event in the Arctic-North Pacific region at MIS 22 (Kender et al., 2018, and this study), is a probable cause for a growth of the LIS at this time, expressed in the discharge of deep erosion products on both the Arctic and North Atlantic side. Another factor contributing to this increased glaciation could be the preceding growth of the perennial sea ice in the western Arctic Ocean, as revealed by a faunal turnover and a decrease in Mn content in P23 during MIS18. Extensive ice cover would have diminished the heat flux from the ocean to the atmosphere even during interglacials when the Bering Strait is open (Cao et al., 2019; van der Linden et al., 2019). More studies, including paleoclimatic modeling experiments, are needed to understand the contributions and linkages of glacial, sea-ice, and sea-level factors.

While the later Pleistocene record in P23 is incomplete due to a core-top loss, available data show very high Ca peaks in glacial intervals since MIS 8, associated with a pronounced glacial isotopic signature (Figs. 2, 4). This pattern is consistent with other, higher-resolution western Arctic records indicating intensified, pulsed glacial inputs from CAA (Dong et al., 2017, 2020; Rong Wang et al., 2021). One possibility for this pattern lies in a progressive erosional deepening and broadening of the CAA straits such as the Amundsen Gulf and M'Clure Strait that connect to extensive exposures of dolomitic rocks (Fig. 1).

An important implication of Bering Strait closures pertains to circulation in the Arctic and adjacent North Atlantic. According to climate modeling experiments (Hu et al., 2012, 2015), lack of exchange across the Bering Strait can affect circulation and deep-water convection as far as the North Atlantic. Hu et al. (2012) conclude that collapse of the Atlantic Meridional Overturning Circulation (AMOC) is only possible when the Bering Strait through-flow is absent or strongly reduced. It is tempting to infer

583 that the Bering Strait closure in MIS 22-24 and subsequent prolonged closures (e.g., MIS
584 16 and 18) contributed to the AMOC collapses that started between MIS 25 and 21 as
585 seen in the South and North Atlantic isotope data (Pena & Goldstein, 2014; Yehudai et
586 al., 2021). This possibility needs to be tested by further paleoclimatic modeling and
587 targeted proxy studies from the AMOC sensitive areas.
588
589 **6. SUMMARY AND CONCLUSIONS**
590 The investigated sediment core P23 from the Northwind Ridge provides the first
591 Arctic record of isotopic provenance tracers across the entire Pleistocene including a
592 distinct depositional shift at the Mid-Pleistocene Transition. Isotopic measurements of
593 detrital Sr and Nd add new insight to earlier conclusions based on litho- and
594 biostratigraphic proxies including elemental Mn and Ca, coarse-grain content, and
595 benthic foraminiferal assemblages. The age framework was developed using
596 lithostratigraphic cyclicity in the glacial part of the record (Unit 1) and Sr isotope
597 stratigraphy in the preglacial Unit 2 extending to estimated ~3.3 Ma. For a broader
598 paleoclimatic background, the P23 data were compared to co-eval isotopic records from
599 the Arctic Ocean and the Bering Sea.
600 The preglacial (upper Pliocene to lower Pleistocene) P23 record is characterized
601 by predominant inputs from the Bering Sea via the Bering Strait and Chukchi shelf, with
602 little to no contributions from glacial sources. A notable exception is a sandy interval in
603 the lower Pleistocene around ~2.5 Ma that bears signs of early Laurentide-like glacial
604 inputs. This isotopic and grain-size composition indicates a limited development of ice
605 sheet(s) in the Canadian Arctic, concurrent with the Cordilleran Ice Sheet that likely
606 exerted a considerable effect on the North Pacific.
607 A steady decrease of ε_{Nd} values towards North American glacigenic signature in
608 both the Arctic and Bering Sea records started at ca. 1.5 Ma, concurrent with a long-term
609 change in oceanic Sr isotopic composition related to glacial erosion. However, the
610 expansion of ice sheet(s) to the Arctic coastline at that time is unlikely as this interval in
611 P23 shows no increase in sand content that would be indicative of iceberg transport.
612 A rapid increase in sedimentary indicators of glacial inputs, started in the Bering
613 Sea at the MPT onset ~1.2-1.3 Ma. In the Arctic Ocean, the major glacigenic threshold

614 expressed in P23 isotope and grain-size proxies was achieved by ~0.9 Ma (MIS22),
615 probably in connection with the first prolonged sea-level drop that closed the Bering
616 Strait for an almost entire obliquity cycle. This change marks an expansion of the North
617 American ice sheets to the Arctic margin, with dramatic impacts on sedimentation and
618 hydrography in the Arctic Ocean. Our record of this major glacial expansion in the Arctic
619 appears to lag behind the North Atlantic, where sedimentary isotopic data indicate an
620 earlier exhaustion of the subglacial regolith and the development of the bedrock-
621 grounded Laurentide Ice Sheet.
622 Isotopic and other proxy data in P23 Unit 1 show that glacigenic impacts on the
623 Arctic Ocean strengthened over the late/post-MPT glacial intervals. The ice-sheet growth
624 was probably enhanced by, and fed-back into, continuing prolonged Bering Strait
625 closures. Another contributing factor could be the spread of perennial sea ice in the
626 western Arctic Ocean, as revealed by a faunal turnover and a decrease in Mn content in
627 P23. Progressing glacial erosion is notably expressed in the increasing inputs of detrital
628 Ca since ~0.65 Ma (MIS 16), with the highest Ca peaks attained ~0.2 Ma later at MIS 8.
629 This pattern may be related to erosional broadening/deepening of the Canadian Arctic
630 straits exposing expansive dolomitic rocks.
631 In addition to the direct effects on the Arctic Ocean climate and hydrography, the
632 Bering Strait closures could have implications for circulation in the North Atlantic as
633 corroborated by modeling studies. The first prolonged Bering Strait closure is co-eval
634 with the first AMOC collapse during the MPT identified in records from the South and
635 North Atlantic. This synchronicity suggests a possible causal relationship that requires
636 further investigation.
637
638

Acknowledgements

- The authors declare that they have no known competing financial interests or personal relationships that could influence the work reported in this paper.
- This work was funded through NSF-ARC grant 1003777/1003740 to L.P. / B.A.H.
- L.P. and B.A.H. were responsible for conceptualization, funding acquisition, and methodology. Resources were provided by L.P. (samples) and B.A.H. (reagents, instrumentation). J.M.M., B.A.H., and A.K. conducted the investigation. Writing: J.M.M. wrote the initial draft, J.M.M., L.P., and B.A.H. performed review & editing. J.M.M. curated the data.

Open Research

All data associated with this publication will be found online at Pangaea Data Publisher (pangaea.de). The digital object identifier will be provided when it is assigned.

REFERENCES

Abbott, A. N., Haley, B. A., & McManus, J. (2016). The impact of sedimentary coatings on the diagenetic Nd flux. *Earth and Planetary Science Letters*, *449*, 217–227. https://doi.org/10.1016/j.epsl.2016.06.001

Asahara, Y., Takeuchi, F., Nagashima, K., Harada, N., Yamamoto, K., Oguri, K., & Tadai, O. (2012). Provenance of terrigenous detritus of the surface sediments in the Bering and Chukchi Seas as derived from Sr and Nd isotopes: Implications for recent climate change in the Arctic regions. *Deep-Sea Research II*, *61–64*, 155–171. https://doi.org/10.1016/j.dsr2.2011.12.004

Balco, G., & Rovey II, C. W. (2010). Absolute chronology for major Pleistocene advances of the Laurentide Ice Sheet. *Geology*, *38*(9), 795–798. https://doi.org/10.1130/G30946.1

Batchelor, C. L., Margold, M., Krapp, M., Murton, D. K., Dalton, A. S., Gibbard, P. L., et al. (2019). The configuration of Northern Hemisphere ice sheets through the Quaternary. *Nature Communications*, *10*(3713). https://doi.org/10.1038/s41467-019-11601-2

Bazhenova, E., Fagel, N., & Stein, R. (2017). North American origin of "pink-white" layers at the Mendeleev Ridge (Arctic Ocean): New insights from lead and neodymium isotope composition of detrital sediment component. *Marine Geology*, *386*, 44–55. https://doi.org/10.1016/j.margeo.2017.01.010

Bischof, J. F., & Darby, D. A. (1997). Mid- to Late Pleistocene Ice Drift in the Western Arctic Ocean: Evidence for a Different Circulation in the Past. *Science*, *277*(5322), 74–78. https://doi.org/10.1126/science.277.5322.74

Borg, L. E., & Banner, J. L. (1996). Neodymium and strontium isotopic constraints on soil sources in Barbados, West Indies. *Geochimica et Cosmochimica Acta*, *60*(21), 4193–4206. https://doi.org/10.1016/S0016-7037(96)00252-9

Cao, J., Wang, B., & Liu, J. (2019). Attribution of the Last Glacial Maximum climate formation. *Climate Dynamics*, *53*, 1661–1679. https://doi.org/10.1007/s00382-019-04711-6

Chen, T.-Y., Frank, M., Haley, B. A., Gutjahr, M., & Spielhagen, R. F. (2012). Variations of North Atlantic inflow to the central Arctic Ocean over the last 14 million years inferred from hafnium and neodymium isotopes. *Earth and Planetary Science Letters*, *353–354*, 82–92. https://doi.org/10.1016/j.epsl.2012.08.012

687 Clark, David L., Chern, L. A., Hogler, J. A., Mennicke, C. M., & Atkins, E. D. (1990). Late
688 Neogene climate evolution of the central Arctic Ocean. *Marine Geology*, *93*, 69–
689 94. https://doi.org/10.1016/0025-3227(90)90078-X
690 Clark, D.L., & Hanson, A. (1983). Central Arctic Ocean sediment texture: a key to ice
691 transport mechanisms. In B. F. Molnia (Ed.), *Glacial-marine sedimentation* (pp.
692 301–330). New York and London: Plenum Press.
693 Clark, P. U., & Pollard, D. (1998). Origin of the middle Pleistocene transition by ice sheet
694 erosion of regolith. *Paleoceanography*, *13*(1), 1–9.
695 https://doi.org/10.1029/97PA02660
696 Clark, P. U., Archer, D., Pollard, D., Blum, J. D., Rial, J. A., Brovkin, V., et al. (2006). The
697 middle Pleistocene transition: characteristics, mechanisms, and implications for
698 long-term changes in atmospheric pCO2. *Quaternary Science Reviews*, *25*, 3150–
699 3184. https://doi.org/10.1016/j.quascirev.2006.07.008
700 Cronin, T. M., Polyak, L., Reed, D., Kandiano, E. S., Marzen, R. E., & Council, E. A. (2013).
701 A 600-ka Arctic sea-ice record from Mendeleev Ridge based on ostracodes.
702 *Quaternary Science Reviews*, *79*, 157–167.
703 https://doi.org/10.1016/j.quascirev.2012.12.010
704 Darby, D. A. (2008). Arctic perennial ice cover over the last 14 million years.
705 *Paleoceanography*, *23*(1). https://doi.org/10.1029/2007PA001479
706 Darby, D. A., Myers, W. B., Jakobsson, M., & Rigor, I. (2011). Modern dirty sea ice
707 characteristics and sources: The role of anchor ice. *Journal of Geophysical*
708 *Research*, *116*, C09008. https://doi.org/10.1029/2010JC006675

709 Dethleff, D. (2005). Entrainment and export of Laptev Sea ice sediments, Siberian Arctic.
710 *Journal of Geophysical Research*, *110*, C07009.
711 https://doi.org/10.1029/2004JC002740
712 Dipre, G. R., Polyak, L., Kuznetsov, A. B., Oti, E. A., Ortiz, J. D., Brachfeld, S. A., et al.
713 (2018). Plio-Pleistocene sedimentary record from the Northwind Ridge: new
714 insights into paleoclimatic evolution of the western Arctic Ocean for the last 5
715 Ma. *Arktos*, *4*(24). https://doi.org/10.1007/s41063-018-0054-y
716 Dong, L., Liu, Y., Shi, X., Polyak, L., Huang, Y., Fang, X., et al. (2017). Sedimentary record
717 from the Canada Basin, Arctic Ocean: implications for late to middle Pleistocene
718 glacial history. *Climate of the Past*, *13*, 511–531. https://doi.org/10.5194/cp-13-
719 511-2017
720 Dong, L., Polyak, L., Liu, Y., Shi, X., Zhang, J., & Huang, Y. (2020). Isotopic Fingerprints of
721 Ice-Rafted Debris Offer New Constraints on Middle to Late Quaternary Arctic
722 Circulation and Glacial History. *Geochemistry, Geophysics, Geosystems*, *21*,
723 e2020GC009019. https://doi.org/10.1029/2020GC009019
724 Duk-Rodkin, A., Barendregt, R. W., White, J. M., & Singhroy, V. H. (2001). Geologic
725 evolution of the Yukon River: implications for placer gold. *Quaternary*
726 *International*, *82*, 5–31. https://doi.org/10.1016/S1040-6182(01)00006-4
727 Dyke, A. S., Moore, A., & Robertson, L. (2003). Deglaciation of North America. Natural
728 Resources Canada.
729 Eisenhauer, A., Meyer, H., Rachold, V., Tütken, T., Wiegand, B., Hansen, B. T., et al.
730 (1999). Grain size separation and sediment mixing in Arctic Ocean sediments:

731 evidence from the strontium isotope systematic. *Chemical Geology*, *158*, 173–
732 188. https://doi.org/10.1016/S0009-2541(99)00026-1
733 Elderfield, H., Ferretti, P., Greaves, M., Crowhurst, S., McCave, I. N., Hodell, D., &
734 Piotrowski, A. M. (2012). Evolution of Ocean Temperature and Ice Volume
735 Through the Mid-Pleistocene Climate Transition. *Science*, *337*(6095), 704–709.
736 https://doi.org/10.1126/science.1221294
737 Fagel, N., Not, C., Gueibe, J., Mattielli, N., & Bazhenova, E. (2014). Late Quaternary
738 evolution of sediment provenances in the Central Arctic Ocean: mineral
739 assemblage, trace element composition and Nd and Pb isotope fingerprints of
740 detrital fraction from the Northern Mendeleev Ridge. *Quaternary Science*
741 *Reviews*, *92*, 140–154. https://doi.org/10.1016/j.quascirev.2013.12.011
742 Gamboa, A., Montero-Serrano, J.-C., St-Onge, G., Rochon, A., & Desiage, P.-A. (2017).
743 Mineralogical, geochemical, and magnetic signatures of surface sediments from
744 the Canadian Beaufort Shelf and Amundsen Gulf (Canadian Arctic).
745 *Geochemistry, Geophysics, Geosystems*, *18*(2), 488–512.
746 https://doi.org/10.1002/2016GC006477
747 Haley, B. A., Frank, M., Spielhagen, R. F., & Eisenhauer, A. (2008). Influence of brine
748 formation on Arctic Ocean circulation over the past 15 million years. *Nature*
749 *Geoscience*, *1*(1), 68–72. https://doi.org/10.1038/ngeo.2007.5
750 Haley, B. A., Frank, M., Spielhagen, R. F., & Fietzke, J. (2008). Radiogenic isotope record
751 of Arctic Ocean circulation and weathering inputs of the past 15 million years.
752 *Paleoceanography*, *23*(1). https://doi.org/10.1029/2007PA001486

753 Hidy, A. J., Gosse, J. C., Froese, D. G., Bond, J. D., & Rood, D. H. (2013). A latest Pliocene
754 age for the earliest and most extensive Cordilleran Ice Sheet in northwestern
755 Canada. *Quaternary Science Reviews*, *61*, 77–84.
756 https://doi.org/10.1016/j.quascirev.2012.11.009
757 Hillaire-Marcel, C., Maccali, J., Not, C., & Poirier, A. (2013). Geochemical and isotopic
758 tracers of Arctic sea ice sources and export with special attention to the Younger
759 Dryas interval. *Quaternary Science Reviews*, *79*, 184–190.
760 https://doi.org/10.1016/j.quascirev.2013.05.001
761 Hodell, D. A., Channell, J. E. T., Curtis, J. H., Romero, O. E., & Röhl, U. (2008). Onset of
762 "Hudson Strait" Heinrich events in the eastern North Atlantic at the end of the
763 middle Pleistocene transition (~640 ka)? *Paleoceanography*, *23*.
764 https://doi.org/10.1029/2008PA001591
765 Hönisch, B., Hemming, N. G., Archer, D., Siddall, M., & McManus, J. F. (2009).
766 Atmospheric Carbon Dioxide Concentration Across the Mid-Pleistocene
767 Transition. *Science*, *324*(5934), 1551–1554.
768 https://doi.org/10.1126/science.1171477
769 Horikawa, K., Asahara, Y., Yamamoto, K., & Okazaki, Y. (2010). Intermediate water
770 formation in the Bering Sea during glacial periods: Evidence from neodymium
771 isotope ratios. *Geology*, *38*(5), 435–438. https://doi.org/10.1130/G30225.1
772 Horikawa, K., Martin, E. E., Basak, C., Onodera, J., Seki, O., Sakamoto, T., et al. (2015).
773 Pliocene cooling enhanced by flow of low-salinity Bering Sea water to the Arctic
774 Ocean. *Nature Communications*, *6*, 7587. https://doi.org/10.1038/ncomms8587

Hu, A., Meehl, G. A., Han, W., Abe-Ouchi, A., Morrill, C., Okazaki, Y., & Chikamoto, M. O. (2012). The Pacific-Atlantic seesaw and the Bering Strait. *Geophysical Research Letters*, *39*. https://doi.org/10.1029/2011GL050567

Hu, A., Meehl, G. A., Han, W., Otto-Bliestner, B., Abe-Ouchi, A., & Rosenbloom, N. (2015). Effects of the Bering Strait closure on AMOC and global climate under different background climates. *Progress in Oceanography*, *132*, 174–196. https://doi.org/10.1016/j.pocean.2014.02.004

Jakobsson, M., Løvlie, R., Al-Hanbali, H., Arnold, E., Backman, J., & Mörth, M. (2000). Manganese and color cycles in Arctic Ocean sediments constrain Pleistocene chronology. *Geology*, *28*(1), 23–26. https://doi.org/10.1130/0091-7613(2000)28<23:MACCIA>2.0.CO;2

Jakobsson, M., Pearce, C., Cronin, T. M., Backman, J., Anderson, L. G., Barrientos, N., et al. (2017). Post-glacial flooding of the Bering Land Bridge dated to 11 cal ka BP based on new geophysical and sediment records. *Climate of the Past*, *13*, 991–1005. https://doi.org/10.5194/cp-13-991-2017

Jang, K., Huh, Y., & Han, Y. (2017). Authigenic Nd isotope record of North Pacific Intermediate Water formation and boundary exchange on the Bering Slope. *Quaternary Science Reviews*, *156*, 150–163. https://doi.org/10.1016/j.quascirev.2016.11.032

Kaufman, D. S., Young, N. E., Briner, J. P., & Manley, W. F. (2011). Alaska Palaeo-Glacier Atlas (Version 2). In J. Ehlers, P. L. Gibbard, & P. D. Hughes (Eds.), *Quaternary*

Glaciations - Extent and Chronology: A Closer Look (Vol. 15, pp. 427–445). Elsevier.

Kender, S., Ravelo, A. C., Worne, S., Swann, G. E. A., Leng, M. J., Asahi, H., et al. (2018). Closure of the Bering Strait caused Mid-Pleistocene Transition cooling. *Nature Communications*, *9*(1), 5386. https://doi.org/10.1038/s41467-018-07828-0

Khélifi, N., & Frank, M. (2014). A major change in North Atlantic deep water circulation 1.6 million years ago. *Climate of the Past*, *10*, 1441–1451. https://doi.org/10.5194/cp-10-1441-2014

Kleman, J., Fastook, J., Ebert, K., Nilsson, J., & Caballero, R. (2013). Pre-LGM Northern Hemisphere ice sheet topography. *Climate of the Past*, *9*, 2365–2378. https://doi.org/10.5194/cp-9-2365-2013

Knudson, K. P., & Ravelo, A. C. (2015). North Pacific Intermediate Water circulation enhanced by the closure of the Bering Strait. *Paleoceanography*, *30*, 1287–1304. https://doi.org/10.1002/2015PA002840

Krissek, L. A. (1995). Late Cenozoic ice-rafting records from Leg 145 sites in the North Pacific: late Miocene onset, late Pliocene intensification, and Pliocene-Pleistocene events. In D. K. Rea, I. A. Basov, D. W. Scholl, & J. F. Allan (Eds.), *Proceedings of the Ocean Drilling Program, Scientific Results* (Vol. 145). College Station, TX: Ocean Drilling Program.

Lightfoot, P. C., Hawkesworth, C. J., Hergt, J., Naldrett, A. J., Gorbachev, N. S., Fedorenko, V. A., & Doherty, W. (1993). Remobilisation of the continental lithosphere by a mantle plume: major-, trace-element, and Sr-, Nd-, and Pb-

isotope evidence from picritic and tholeiitic lavas of the Noril'sk District, Siberian Trap, Russia. *Contributions to Mineralogy and Petrology*, *114*, 171–188. https://doi.org/10.1007/BF00307754

van der Linden, E. C., Le Bars, D., Bintanja, R., & Hazeleger, W. (2019). Oceanic heat transport into the Arctic under high and low CO2 forcing. *Climate Dynamics*, *53*, 4763–4780. https://doi.org/10.1007/s00382-019-04824-y

Löwemark, L., März, C., O'Regan, M., & Gyllencreutz, R. (2013). Arctic Ocean Mn-stratigraphy: genesis, synthesis and inter-basin correlation. *Quaternary Science Reviews*, *92*, 97–111. https://doi.org/10.1016/j.quascirev.2013.11.018

Maccali, J., Hillaire-Marcel, C., & Not, C. (2018). Radiogenic isotope (Nd, Pb, Sr) signatures of surface and sea ice-transported sediments from the Arctic Ocean under the present interglacial conditions. *Polar Research*, *37*, 1442982. https://doi.org/10.1080/17518369.2018.1442982

McArthur, J. M., Howarth, R. J., & Shields, G. A. (2012). Strontium Isotope Stratigraphy. In F. Gradstein, J. Ogg, M. Schmitz, & G. Ogg (Eds.), *The Geologic Time Scale* (pp. 127–144). Amsterdam: Elsevier.

McCulloch, M. T., & Wasserburg, G. J. (1978). Sm-Nd and Rb-Sr Chronology of Continental Crust Formation. *Science*, *200*(4345), 1003–1011. https://doi.org/10.1126/science.200.4345.1003

Moran, K., Backman, J., Brinkhuis, H., Clemens, S. C., Cronin, T., Dickens, G. R., et al. (2006). The Cenozoic palaeoenvironment of the Arctic Ocean. *Nature*, *441*, 601–605. https://doi.org/10.1038/nature04800

840 Muratli, J. M., McManus, J., Mix, A., & Chase, Z. (2012). Dissolution of fluoride
841 complexes following microwave-assisted hydrofluoric acid digestion of
842 sediments. *Talanta*, *89*, 195–200. https://doi.org/10.1016/j.talanta.2011.11.081
843 Niessen, F., Hong, J. K., Hegewald, A., Matthiessen, J., Stein, R., Kim, H., et al. (2013).
844 Repeated Pleistocene glaciation of the East Siberian continental margin. *Nature*
845 *Geoscience*, *6*, 842–846. https://doi.org/10.1038/NGEO1904
846 Nürnberg, D., Wollenburg, I., Dethleff, D., Eicken, H., Kassens, H., Letzig, T., et al. (1994).
847 Sediments in Arctic sea ice: Implications for entrainment, transport and release.
848 *Marine Geology*, *119*, 185–214. https://doi.org/10.1016/0025-3227(94)90181-3
849 O'Regan, M., King, J., Backman, J., Jakobsson, M., Pälike, H., Moran, K., et al. (2008).
850 Constraints on the Pleistocene chronology of sediments from the Lomonosov
851 Ridge. *Paleoceanography*, *23*(PA1S19). https://doi.org/10.1029/2007PA001551
852 Pena, L. D., & Goldstein, S. L. (2014). Thermohaline circulation crisis and impacts during
853 the mid-Pleistocene transition. *Science*, *345*(6194), 318–322.
854 https://doi.org/10.1126/science.1249770
855 Poirier, R. K., & Billups, K. (2014). The intensification of northern component deepwater
856 formation during the mid-Pleistocene climate transition. *Paleoceanography*, *29*,
857 1046–1061. https://doi.org/10.1002/2014PA002661
858 Polyak, L., Bischof, J., Ortiz, J. D., Darby, D. A., Channell, J. E. T., Xuan, C., et al. (2009).
859 Late Quaternary stratigraphy and sedimentation patterns in the western Arctic
860 Ocean. *Global and Planetary Change*, *68*, 5–17.
861 https://doi.org/10.1016/j.gloplacha.2009.03.014

862 Polyak, L., Best, K. M., Crawford, K. A., Council, E. A., & St-Onge, G. (2013). Quaternary
863 history of sea ice in the western Arctic Ocean based on foraminifera. *Quaternary*
864 *Science Reviews*, *79*, 145–156. https://doi.org/10.1016/j.quascirev.2012.12.018
865 Porcelli, D., Andersson, P. S., Baskaran, M., Frank, M., Björk, G., & Semiletov, I. (2009).
866 The distribution of neodymium isotopes in Arctic Ocean basins. *Geochimica et*
867 *Cosmochimica Acta*, *73*, 2645–2659. https://doi.org/10.1016/j.gca.2008.11.046
868 Rohling, E. J., Foster, G. L., Grant, K. M., Marino, G., Roberts, A. P., Tamisiea, M. E., &
869 Williams, F. (2014). Sea-level and deep-sea-temperature variability over the past
870 5.3 million years. *Nature*, *508*, 477–482. https://doi.org/10.1038/nature13230
871 Shakun, J. D., Raymo, M. E., & Lea, D. W. (2016). An early Pleistocene Mg/Ca-d18O
872 record from the Gulf of Mexico: Evaluating ice sheet size and pacing in the 41-kyr
873 world. *Paleoceanography*, *31*, 1011–1027.
874 https://doi.org/10.1002/2016PA002956
875 Sharma, M., Basu, A. R., & Nesterenko, G. V. (1992). Temporal Sr-, Nd-, and Pb-isotopic
876 variations in the Siberian flood basalts: Implications for the plume-source
877 characteristics. *Earth and Planetary Science Letters*, *113*(3), 365–381.
878 https://doi.org/10.1016/0012-821X(92)90139-M
879 Shimada, K., Kamoshida, T., Itoh, M., Nishino, S., Carmack, E., McLaughlin, F., et al.
880 (2006). Pacific Ocean inflow: Influence on catastrophic reduction of sea ice cover
881 in the Arctic Ocean. *Geophysical Research Letters*, *33*, L08605.
882 https://doi.org/10.1029/2005GL025624

Spada, G., & Galassi, G. (2017). Extent and dyamic evolution of the lost land aquaterra since the Last Glacial Maximum. *Comptes Rendus Geoscience*, *349*, 151–158. https://doi.org/10.1016/j.crte.2017.06.004

Stärz, M., Gong, X., Stein, R., Darby, D. A., Kauker, F., & Lohmann, G. (2012). Glacial shortcut of Arctic sea-ice transport. *Earth and Planetary Science Letters*, *357–358*, 257–267. https://doi.org/10.1016/j.epsl.2012.09.033

Stein, R., Matthiessen, J., & Niessen, F. (2010). Re-Coring at Ice Island T3 Site of Key Core FL-224 (Nautilus Basin, Amerasian Arctic): Sediment Characteristics and Stratigraphic Framework. *Polarforschung*, *79*(2), 81–96. https://doi.org/10.2312/polarforschung.79.2.81

Stein, R., Matthiessen, J., Niessen, F., Krylov, A., Nam, S., & Bazhenova, E. (2010). Towards a Better (litho-) Stratigraphy and Reconstruction of Quaternary Paleoenvironment in the Amerasian Basin (Arctic Ocean). *Polarforschung*, *79*(2), 97–121. https://doi.org/10.2312/polarforschung.79.2.97

Stein, R., Fahl, K., & Müller, J. (2012). Proxy Reconstruction of Cenozoic Arctic Ocean Sea-Ice History – from IRD to IP25. *Polarforschung*, *82*(1), 37–71. https://doi.org/10.2312/polarforschung.82.1.37

Stokes, C. R., Clark, C. D., Darby, D. A., & Hodgson, D. A. (2005). Late Pleistocene ice export events into the Arctic Ocean from the M'Clure Strait Ice Stream, Canadian Arctic Archipelago. *Global and Planetary Change*, *49*, 139–162. https://doi.org/10.1016/j.gloplacha.2005.06.001

Studer, A. S., Martínez-Garcia, A., Jaccard, S. L., Girault, F. E., Sigman, D. M., & Haug, G. H. (2012). Enhanced stratification and seasonality in the Subarctic Pacific upon Northern Hemisphere Glaciation – New evidence from diatom-bound nitrogen isotopes, alkenones and archaeal tetraethers. *Earth and Planetary Science Letters*, *351–352*, 84–94. https://doi.org/10.1016/j.epsl.2012.07.029

Svendsen, J. I., Alexanderson, H., Astakhov, V. I., Demidov, I., Dowdeswell, J. A., Funder, S., et al. (2004). Late Quaternary ice sheet history of northern Eurasia. *Quaternary Science Reviews*, *23*, 1229–1271. https://doi.org/10.1016/j.quascirev.2003.12.008

Tanaka, T., Togashi, S., Kamioka, H., Amakawa, H., Kagami, H., Hamamoto, T., et al. (2000). JNdi-1: a neodymium isotopic reference in consistency with LaJolla neodymium. *Chemical Geology*, *168*(3–4), 279–281. https://doi.org/10.1016/S0009-2541(00)00198-4

Tikhomirov, P. L., Kalinina, E. A., Kobayashi, K., & Nakamura, E. (2008). Late Mesozoic silicic magmatism of the North Chukotka area (NE Russia): Age, magma sources, and geodynamic implications. *Lithos*, *105*, 329–346. https://doi.org/10.1016/j.lithos.2008.05.005

Tütken, T., Eisenhauer, A., Wiegand, B., & Hansen, B. T. (2002). Glacial-interglacial cycles in Sr and Nd isotopic composition of Arctic marine sediments triggered by the Svalbard/Barents Sea ice sheet. *Marine Geology*, *182*(3–4), 351–372. https://doi.org/10.1016/S0025-3227(01)00248-1

925 Walczak, M. H., Mix, A. C., Cowan, E. A., Fallon, S., Fifield, L. K., Alder, J. R., et al. (2020).
926 Phasing of millenial-scale climate variability in the Pacific and Atlantic Oceans.
927 *Science*, *370*(6517), 716–720. https://doi.org/10.1126/science.aba7096
928 Wang, Rong, Polyak, L., Zhang, W., Yu, X., Ye, L., Dong, L., et al. (2021). Glacial-
929 interglacial sedimentation and paleocirculation at the Northwind Ridge, western
930 Arctic Ocean. *Quaternary Science Reviews*, *258*, 106882.
931 https://doi.org/10.1016/j.quascirev.2021.106882
932 Wang, Rujian, Polyak, L., Xiao, W., Wu, L., Zhang, T., Sun, Y., & Xu, X. (2018). Late-Middle
933 Quaternary lithostratigraphy and sedimentation patterns on the Alpha Ridge,
934 central Arctic Ocean: Implications for Arctic climate variability on orbital time
935 scales. *Quaternary Science Reviews*, *181*, 93–108.
936 https://doi.org/10.1016/j.quascirev.2017.12.006
937 Wasserburg, G. J., Jacobsen, S. B., DePaolo, D. J., McCulloch, M. T., & Wen, T. (1981).
938 Precise determination of Sm/Nd ratios, Sm and Nd isotopic abundances in
939 standard solutions. *Geochimica et Cosmochimica Acta*, *45*(12), 2311–2323.
940 https://doi.org/10.1016/0016-7037(81)90085-5
941 Winter, B. L., Johnson, C. M., & Clark, D. L. (1997). Strontium, neodymium, and lead
942 isotope variations of authigenic and silicate sediment components from the Late
943 Cenozoic Arctic Ocean: Implications for sediment provenance and the source of
944 trace metals in seawater. *Geochimica et Cosmochimica Acta*, *61*(19), 4181–4200.
945 https://doi.org/10.1016/S0016-7037(97)00215-9

946 Wooden, J. L., Czamanske, G. K., Fedorenko, V. A., Arndt, N. T., Chauvel, C., Bouse, R. M.,
947 et al. (1993). Isotopic and trace-element constraints on mantle and crustal
948 contributions to Siberian continental flood basalts, Noril'sk area, Siberia.
949 *Geochimica et Cosmochimica Acta*, *57*(15), 3677–3704.
950 https://doi.org/10.1016/0016-7037(93)90149-Q
951 Xiao, W., Polyak, L., Wang, R., Not, C., Dong, L., Liu, Y., et al. (2021). A sedimentary
952 record from the Makarov Basin, Arctic Ocean, reveals changing middle to Late
953 Pleistocene glaciation patterns. *Quaternary Science Reviews*, *270*, 107176.
954 https://doi.org/10.1016/j.quascirev.2021.107176
955 Yamamoto, M., Nam, S.-I., Polyak, L., Kobayashi, D., Suzuki, K., Irino, T., & Shimada, K.
956 (2017). Holocene dynamics in the Bering Strait inflow to the Arctic and the
957 Beaufort Gyre circulation based on sedimentary records from the Chukchi Sea.
958 *Climate of the Past*, *13*, 1111–1127. https://doi.org/10.5194/cp-13-1111-2017
959 Yehudai, M., Kim, J., Pena, L. D., Jaume-Seguí, M., Knudson, K. P., Bolge, L., et al. (2021).
960 Evidence for a Northern Hemispheric trigger of the 100,000-y glacial cyclicity.
961 *Proceedings of the National Academy of Sciences*, *118*(46), e2020260118.
962 https://doi.org/10.1073/pnas.2020260118
963 Yurco, L. N., Ortiz, J. D., Polyak, L., Darby, D. A., & Crawford, K. A. (2010). Clay mineral
964 cycles identified by diffuse spectral reflectance in Quaternary sediments from
965 the Northwind Ridge: implications for glacial-interglacial sedimentation patterns
966 in the Arctic Ocean. *Polar Research*, *29*, 176–197.
967 https://doi.org/10.1111/j.1751-8369.2010.00160.x

968 Zachos, J., Pagani, M., Sloan, L., Thomas, E., & Billups, K. (2001). Trends, Rhythms, and
969 Aberrations in Global Climate 65 Ma to Present. *Science*, *292*(5517), 686–693.
970 https://doi.org/10.1126/science.1059412

971